Ann Biomed Eng 47, 1799–1814 (2019). https://doi.org/10.1007/s10439-019-02273-6

Left ventricular hemodynamics with an implanted assist device: an in-vitro fluid dynamics study

Francesco Viola[1], Elizabeth Jermyn[2], James Warnock[3], Giorgio Querzoli[4] and Roberto Verzicco[1,5]

affiliations: [1] PoF, UTwente, Drienerlolaan 5 7522NB Enschede, The Netherlands

affiliations: [2] Department of Agricultural and Biological Engineering, Mississippi State University, Mississippi State, MS 39759

affiliations: [3] School of Chemical, Materials, and Biomedical Engineering, University of Georgia, Athens, GA 30602

affiliations: [4] DICAAR, University of Cagliari, Via Marengo, 2, 09123 Cagliari, Italy

affiliations: [5] Department of Industrial Engineering, University of Roma Tor Vergata, Italy

abbreviated title: Left ventricular hemodynamics with an implanted assist device: an in-vitro fluid dynamics study

correspondence: PoF, UTwente, Drienerlolaan 5 7522NB Enschede, The Netherlands.
e-mail: f.viola@utwente.nl

Abstract

Left ventricle assist devices (VADs) aid the heart pumping blood into the systemic circulation and grant the required cardiac output (CO) when the heart itself cannot provide it. However, it is unclear how effective these devices are at restoring not only physiological CO values but also normal intraventricular hemodynamics.

In this work, the modified hemodynamics due to a VAD implantation is studied in-vitro using an elastic ventricle made of silicone, which is incorporated into a pulse-duplicator setup prescribing a realistic pulsatile flow. Thereafter, a continuous axial pump is connected at the ventricle apex to mimic a VAD and its effect on the ventricular hemodynamics is investigated as a function of the pump flow suction. Using particle image velocimetry (PIV), we observe that the continuous pump flow effectively provides unloading on the ventricle and yields an increased CO. Conversely, the continuous blood suction from the ventricle apex deeply alters the hemodynamics and, in addition, the VAD obstruction in the ventricle behaves as a bluff body that affects the vorticity distribution in the LV thus creating a stagnant region at the ventricle apex. This phenomenon is rationalized by measuring in a modified set-up the benefits on the hemodynamics of a flush-mounted device. Additionally, the suction operated by the VAD reduces the ventricular pressure and yields an increase in the swirling motion around the ventricle axis, in a similar fashion as the bath-tub vortex effect, thus further modifying the intraventricular hemodynamics with respect to healthy conditions.

1 Introduction

Dilated cardiomyopathy (DCM) is a progressive disease of the heart muscle that is characterized by contractile dysfunction and ventricular chamber enlargement, as sketched in Figure 1. As the myocardium becomes damaged, the tissue weakens and the left ventricle (LV) is unable to function on its own. As a result, the cardiac output (CO), quantifies the pumping efficiency of the ventricle and is defined as the blood volume delivered by the LV in a minute, reduces [1,2]. DCM can also cause other pathologies such as the formation of blood clots and heart valve problems and, consequently, is the third most common cause of heart failure and the most frequent reason for heart transplantation [1,3]. Unfortunately, the number of available donor hearts is inadequate to satisfy this demand (more than 70,000 people each year [4]) and many patients need a ventricular assist device (VAD) to aid the ventricles pumping blood [5].

Left ventricular assist devices (VADs) are pumps [6,7] implanted at the ventricle apex in order to provide the necessary unloading of the LV in patients experiencing some form of heart failure due to LV dysfunction (see Figure 1c). Continuous-flow VAD supply an average cardiac output of 4 l/min with a maximum of 8 l/min [8,9,10], which is within the physiological cardiac output range [2]. These devices are used in end-stage heart failure patients, typically as a bridge to transplant [9], or as a destination therapy if the patient is untreatable [11]. However, as the average duration of long-term support increases, device performance in terms of hemodynamics becomes an increasing contributor to patient survival, and advances in technology are expected to improve long-term outcomes and living quality of the patients [12,7].

Despite the fact that VADs increase the CO to acceptable ranges, patients with VADs are prescribed the additional use of anticoagulants in order to reduce the likelihood of further complications such as clots formation [13,14,15]. The reason why VADs also require further medication is generally related to the altered hemodynamics and its effect on the proper flushing of the myocardium [20], which is the main focus of this study. To investigate these aspects we perform a series of in-vitro experiments using a simplified LV model connected to a cardiovascular pulse-duplicator [17,18,19], designed to reproduce temporal variations of the ventricle volume similar to

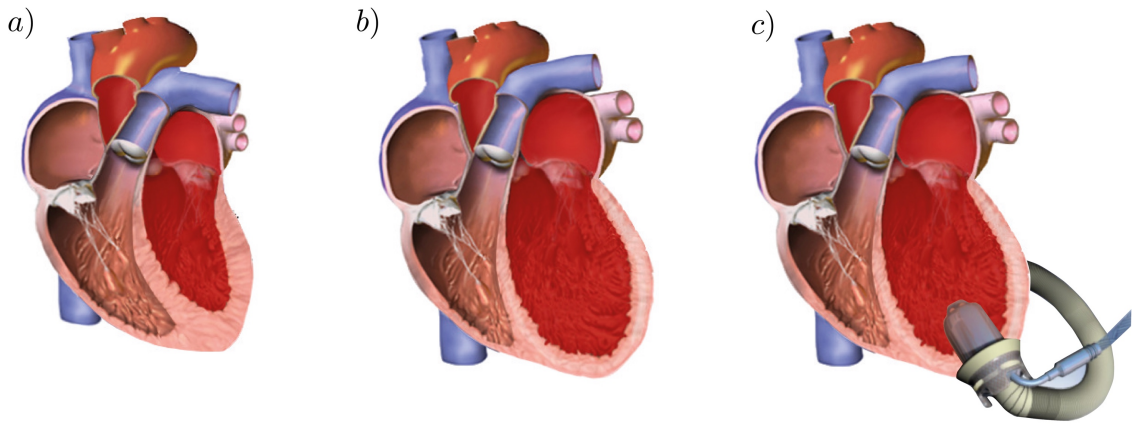

Figure 1: Anatomical slice of the human heart[21] (a) in normal conditions (b) affected by DCM and (c) with a VAD implanted.

those observed in the human heart in low EF conditions. Thereafter, a continuous axial pump is connected at the ventricle apex to mimic a VAD, and its effect on the ventricular hemodynamics is investigated using particle image velocimetry (PIV). This work aims at studying how the physiological hemodynamics in the LV changes, when a VAD is implanted, in terms of kinetic energy of the blood flow and intraventricular vortex dynamics as a function of the VAD flow-rate. In particular, the proper washout of the myocardium and the appearance of stagnant region is monitored as a potential risk for clots formation. Furthermore, the effect of the VAD obstruction within the left ventricle is investigated in the limit case of a flush-mounted VAD.

2 Materials and methods

The cardiovascular pulse-duplicator

A cardiovascular pulse-duplicator, as shown in Figure 2, is used to replicate the dynamics in the LV of the heart[22]. The system includes an inverter controller AC electric motor driving a cam that imposes a prescribed displacement in time of a piston/cylinder assembly. This cylinder is connected directly to a rigid transparent plexiglass box containing a synthetic ventricle model made of transparent silicon rubber with embedded silicone-made mitral valve to closely mimic a native valve while a simple check valve is used to model the aortic valve. The LV model is in

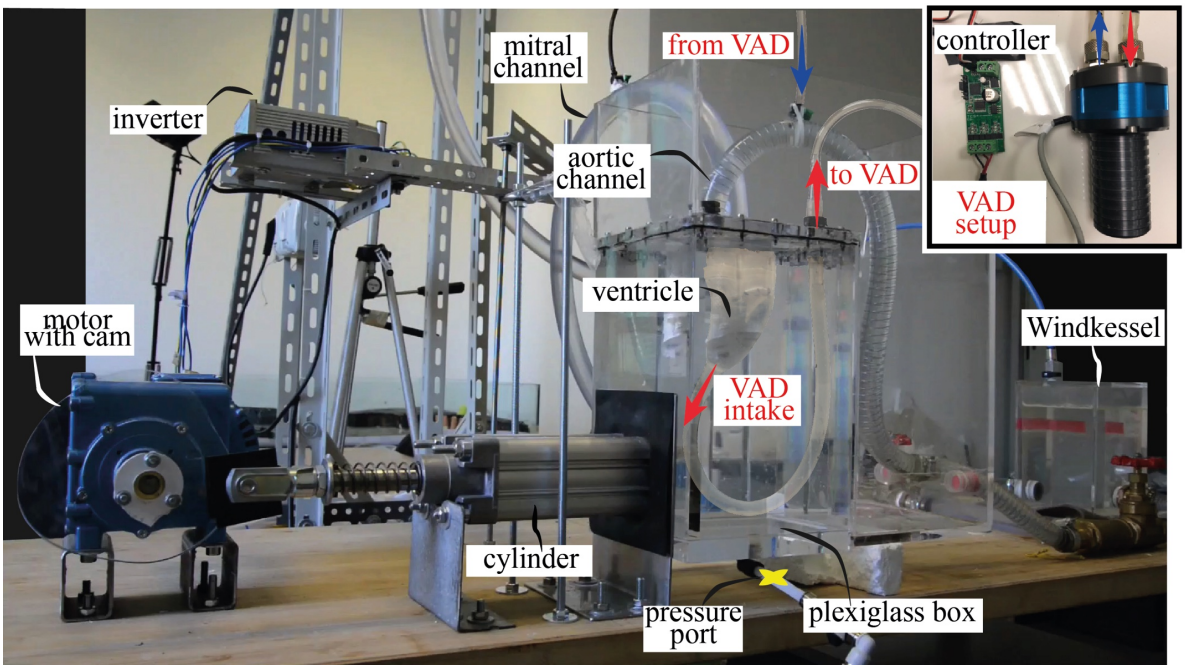

Figure 2: Sketch of the cardiovascular duplicator, where the arrows indicate the VAD flow imposed by the continuous pump, which is shown in the inset.

turn connected to rigid pipes with an inner diameter of 19 mm and 24 mm, respectively, for the aortic and mitral channels. Since the box is filled with the working fluid (deionized water) and sealed, the fluid volume displaced by the piston causes the ventricle to contract (systole) and, consequently pushes fluid into the aortic channel with the prescribed flow rate reported in Figure 3 (red line). Vice-versa when the piston moves away from the box the ventricle expands (diastole) thus sucking water from the mitral channel following the flow rate curve shown in Figure 3 by the green line. Note that the first inflow peak corresponds to the early diastole (the E wave) and the second one to the late diastole (the A wave). Hence, the periodic forward/backward motion of the piston pumps the fluid from the ventricle to the aortic channel, which then flows into the hydraulic loop which includes a Windkessel system, to reproduce the vascular capacitance, and gate valves to regulate the impedance of the systemic circulation (see Figure 2). The fluid after passing through the hydraulic circuit, returns into the ventricle through the mitral duct.

The density of the silicone ($\rho = 1040$ Kg/m^3) is almost identical to the ventricular myocardium (1060 Kg/m^3), and while it is three times stiffer than the tissue of a biological LV ($E = 1.5$ MPa in

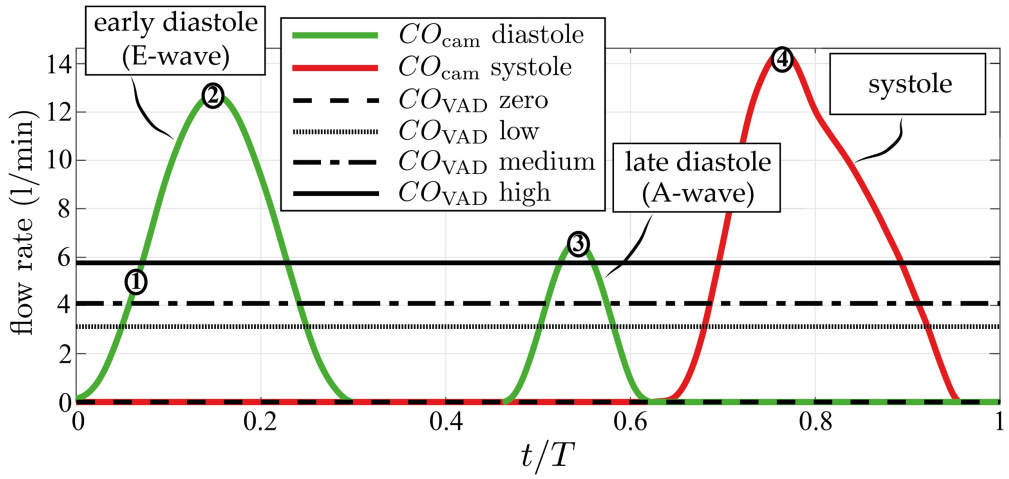

Figure 3: Flow rates versus time, t, normalized using the beating period, T. The non-monotonous curves are the inflow (green line) and outflow (red line) rates imposed by the rotating cam, CO_{cam}, whereas the horizontal lines depict the continuous VAD flow rates CO_{VAD} considered in the experiments. The numbered circles correspond to the acquisition time of the snapshots reported in Figures 6.

the present experiment versus max $E = 0.5$ MPa in the myocardium), it is compensated for by fabricating the ventricle with a thickness equal to one third the one of the myocardium (2-3 mm rather than 6-8 mm). The tele-diastolic volume of the ventricle is set equal to $V_{max} = 220$ ml, so as to reproduce a pathologically dilated heart, whereas its volume variation over a heart beat (stroke) is set by the cam profile to $\Delta V = 40$ ml. Consequently, the tele-systolic volume is $V_{min} = 180$ ml corresponding to an ejection fraction (EF) of

$$EF = \frac{V_{max} - V_{min}}{V_{max}}\% = \frac{\Delta V}{V_{max}}\% = 18.2\%. \tag{1}$$

Blood is a non-Newtonian fluid owing to the surface tension exerted by the suspended cells on the plasma. However, it has been shown that the non-Newtonian blood features become relevant only in vessels of sub-millimeter diameter while in the ventricular flow they produce only minor effects[23,22]. Accordingly, we consider the blood in the ventricle as a Newtonian fluid with an effective viscosity of $\nu = 4.56 \cdot 10^{-6} \text{m}^2\text{s}^{-1}$ (corresponding to a hematocrit of 45%) and a heart rate of HR = 60 beats-per-minute (bpm) that is a typical HR for a healthy human adult.

Consequently, the Reynolds and Womerseley numbers result

$$Re = \frac{\Delta V^{2/3}}{\nu/\omega} = 1611, \qquad Wo = \frac{\Delta V^{1/3}}{\sqrt{\nu/\omega}} = 40.1, \tag{2}$$

being $\omega = 2\pi\mathrm{HR}$ the angular beating frequency of the ventricle. We recall that Re is the ratio between advection and diffusion effects, with high values meaning that the flow is advection dominated in the bulk and that complex flow structures can manifest. On the other hand, Wo is the ratio between the characteristic geometrical length and the size of the oscillating (Stokes) boundary layers at the wall and measures the unsteadiness of the flow. Since the working fluid in the pulse-duplicator is deionized water with a viscosity four times smaller than that of blood, in order to recover the fluid dynamics similarity, the rotation frequency of the cam in the experiment, f, has been reduced by a factor 4 with respect to the HR, $f = \mathrm{HR}/4 = 15$ bpm. In this way the Re and Wo of the experiment attain the same values as in equation (2) and the experiment is thus 'similar' (in the sense of fluid dynamics similarity) to a left heart ventricle beating at $HR = 60$ bpm with a blood of viscosity $\nu = 4.56 \cdot 10^{-6}\mathrm{m}^2\mathrm{s}^{-1}$. As a consequence, the cardiac output produced in the experiment (running with water) is four times smaller than the equivalent CO_{cam} in the case of blood that is defined as

$$CO_{\mathrm{cam}} = \Delta V \text{ x } HR = 40 \text{ ml x } 60 \text{ bpm} = 2.4 \text{ l/min}, \tag{3}$$

which corresponds to life-threatening conditions.

Left ventricular assist device implementation

In order to study the ventricular hemodynamics in presence of a VAD, two model ventricles have been (in-house) manufactured as in Figure 4: (b,c) the first with an attached silicone-rubber tube of 10 mm inner diameter and (a) the second without the tube. The tube reproducing the by-pass duct of VAD has to be flexible enough to follow the ventricle during the contraction but, at the same time, sturdy enough to withstand several cycles of running experiments without detaching from the ventricle. The distal tube end is connected to a centrifugal pump (RS

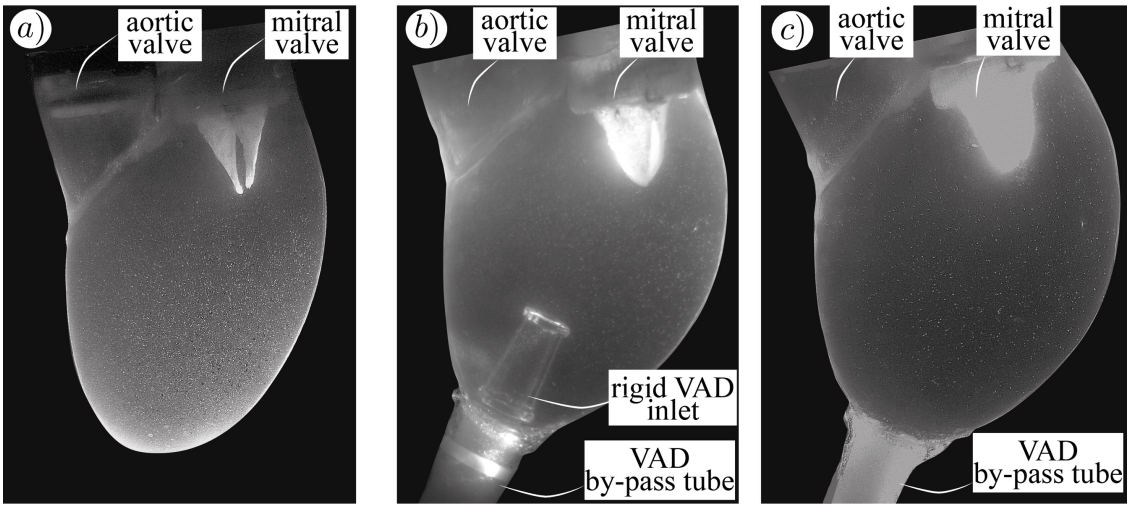

Figure 4: Three experimental configurations: (a) normal, (b) VAD implanted and (c) flush-mounted VAD ventricle.

electronics MG2000) that propels fluid from the ventricle apex to the aortic vessel of the pulse-duplicator, as shown in Figure 2. The pump is controlled by a control board able to accept an input voltage up to 30V DC, while the output voltage can be controlled directly by the on-board speed control potentiometer or using an external 0-5V input. The speed of the pump is driven by an input voltage of 18V as the controller worked to maintain a constant flow rate, in the range $Q_{\mathrm{VAD}} = 13-24$ ml/s, even within time varying pressure differences. In preliminary experiments we have verified that the by-pass flow rate set by the VAD controller is not affected by the pressure loads exerted on the by-pass tube, which is placed inside the plexiglass box containing the ventricle, and that it is insensitive to the cam size and angular frequency (and henceforth on the ventricle ejection fraction and cardiac output). As discussed in the previous paragraph, being the imposed frequency in the experiment, $f = HR/4 = 15$ bpm, the cardiac output of the continuous pump is four times smaller than the equivalent CO_{VAD} in the case of blood that is defined as

$$CO_{\mathrm{VAD}} = Q_{\mathrm{VAD}} \frac{HR}{f} = 4Q_{\mathrm{VAD}}, \tag{4}$$

which varies between 3.1 l/min and 5.8 l/min, as reported in Figure 3. Placing the pump outside the ventricle would correspond to a major modification compared to clinical practice where the VAD pump is often placed inside the ventricle at its apex (see Figure 1c). Hence, in order

to account for the obstruction to the ventricular flow made by the VAD, a rigid plastic inlet of maximum outer diameter 1.5 cm, wall-thickness 1 mm and of length 3.5 cm, which is in the range of typical VAD obstruction in clinical conditions (3-5 cm[24,25]), is placed inside the ventricle. The bottom part of the plastic inlet, which has an outer and inner diameter of 1.2 cm and 1.0 cm, respectively, is inserted directly in the silicone tube as depicted in Figure 4(b).

Particle image velocimetry and pressure measurements

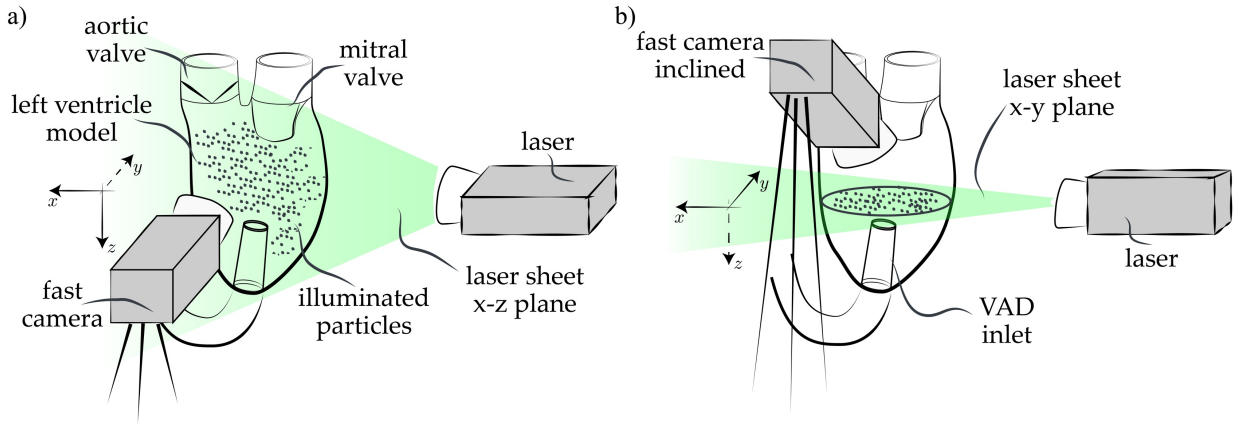

Figure 5: Sketch of the PIV configuration to measure the flow velocity (a) in the symmetry plane of the ventricle, $x-z$, and (b) in the transversal $x-y$ plane above the VAD inlet.

The intraventricular hemodynamics is investigated using Particle Image Velocimetry (PIV) (see Figure 5). The particles used in this experiment are pine pollen, spherical in shape of diameter 50 μm and having the same density as the deionized water. A diode laser is used to emit a high-power beam (≤ 2 W) that is focused using a convergent lens and then spread into a thin sheet through a cylindrical lens. Particle images are recorded by a high-speed camera (Slow Motion Camera Company 1000fps model) equipped with a 256 GB built-in memory and an image resolution of 1280x720 resulting in a spatial resolution of 0.1 mm per pixel. The camera operated at a frame rate of 1000 frames per second and captured the flow for 10 complete heart periods. Data analysis and post-processing is carried out in Matlab using the software PIVlab[26], which is based on a standard cross-correlation method to compute the two-dimensional instantaneous velocity field. The final size of the interrogation windows is 32 x 32 pixels, with a

50 % overlap and a sub-pixel Gaussian interpolation (corresponding to 1.6 mm PIV resolution).

This experimental set-up is used to measure the instantaneous flow velocity in two orthogonal planes within the pulsating ventricle as sketched in Figure 5: (a) the $x-z$ plane, which intersects the VAD inlet at its centerline and the valvular plane at the center of the aortic and mitral orifices, and (b) the $x-y$ plane (orthogonal to the ventricle axis) above the VAD inlet tip. The hemodynamics in the $x-z$ plane is obtained illuminating this plane with the laser sheet and recording the positions of the PIV particles using the fast camera, which is placed orthogonally with respect to the laser sheet, as shown in Figure 5(a). This set-up allows to measure the projection of the velocity vector over the $x-z$ plane, $v_x\mathbf{e}_x+v_z\mathbf{e}_z$, where v_x and v_z are the horizontal and vertical velocity components and $\mathbf{e}_x,\mathbf{e}_z$ the corresponding unit vectors direction. Additionally, the hemodynamics in the transversal plane above the VAD inlet (Figure 5b) are measured by rotating the cylindrical lens with respect the previous configuration so that the laser sheet is orthogonal to the ventricle main axis. In this case, the camera can not be placed orthogonal to the laser sheet since the optical path is obstructed by the mitral and aortic channels (see Figure 2). Hence, the camera is inclined by 45° about the x axis so that instantaneous position of the PIV particles can be conveniently recorded and the velocity data corrected in the post-processing to account for the camera inclination and refraction index differences, thus yielding the velocity vector projected over the $x-y$ plane, $v_x\mathbf{e}_x+v_y\mathbf{e}_y$.

The cardiovascular pulse-duplicator is equipped with a pressure port for measuring the absolute pressure inside the plexiglass box containing the beating ventricle (see the yellow 'x' symbol in Figure 2). The port has an outer tip, which is directly connected to a piezoresistive silicon pressure sensor (Honeywell TruStability^{TM}) with an accuracy of $\pm 0.25\%$ in the range of 0-1.6 bar. The sensor is controlled by an Arduino UNO system, which receives the analogical output voltage from the sensor and converts it to pressure data through the calibration curve provided by the manufacturer.

$\mathbf{CO_{VAD}}$	equivalent HR (bpm)	cam stroke (ml)	equivalent $\mathbf{CO_{cam}}$(l/min)	equivalent $\mathbf{CO_{VAD}}$(l/min)	equivalent $\mathbf{CO_{tot}}$ (l/min)	$\mathbf{R_{CO}}$
zero	60	40	2.4	0.0	2.4	0
low	60	40	2.4	3.1	5.5	1.3
medium	60	40	2.4	4.1	6.5	1.7
high	60	40	2.4	5.8	8.2	2.4

Table 1: Parameters of the experiments.

3 Results

Three different configurations have been investigated in our experiments as shown in Figure 4: (i) ventricle without VAD (ii) VAD mounted inside the ventricle and (iii) flush-mounted VAD. Experimental results for configuration (ii), which better reproduces a realistic VAD-like ventricle accounting for the VAD blockage on the flow, are first reported. Hemodynamics variations with respect to the configurations (i) and (iii) are then discussed.

3.1 VAD modified cardiac output

Let us consider an impaired ventricle with a low cardiac output and investigate the VAD capability at restoring a healthy physiological blood delivery. Four VAD regimes can be studied by varying the by-pass flow rate, namely *zero* (VAD turned off), *low* (CO_{VAD} = 3.1 l/min), *medium* (CO_{VAD} = 4.1 l/min) and *high* (CO_{VAD} = 5.8 l/min), which are reported in Figure 3 and in Table 1. When the VAD is active, the net liquid volume ejected from the ventricle during a heart beat increases. As a consequence, it is possible to define a VAD-modified cardiac output, CO_{tot}, to account for the continuous by-pass flow as follows:

$$CO_{\mathrm{tot}} = CO_{\mathrm{cam}} + CO_{\mathrm{VAD}}, \tag{5}$$

where CO_{cam} is the equivalent cardiac output only due to the piston and is here set to 2.4 l/min (see equation 3). This low cardiac output corresponds to life threatening conditions and is kept fixed throughout all experiments. CO_{VAD} is due to the VAD suction, and R_{CO} is the ratio between

the two, i.e. $R_{CO} = CO_{\text{VAD}}/CO_{\text{cam}}$. The latter is a measure of the VAD blood delivery with respect to that due to the active LV contraction. The total cardiac output CO_{tot}, defined in equation (5), depends on the VAD pumping as reported in Table 1, and the increase in VAD flow rate directly correlates with an improvement in the cardiac output towards the normal physiological range. In particular, the low flow-rate configuration yields a CO_{tot} of 5.5 l/min, which increases up to 6.5 l/min when the VAD is set at the medium flow-rate. The total cardiac output is more than doubled with respect the nominal CO_{cam}, thus modifying the pumping ability of the heart from 'severely below normal' to 'normal', according to the American Heart society standards[3]. Furthermore, when the VAD suction is set to high flow-rate the ratio R_{CO} gets to 2.4, meaning that the VAD pumping is more than twice more effective than the LV active contraction. Hence, the total cardiac output, CO_{tot}, exceeds 8 l/min, which corresponds to a relevant blood pumping for a healthy subject.

3.2 Ventricular hemodynamics with an implanted assist device

The VAD efficacy, however, can not be assessed only through an integral quantity such as the total cardiac output CO_{tot}, since also the resulting intraventricular hemodynamics has to be monitored. To this aim, Figure 6 shows the $x-z$ velocity during systole and diastole as a function of the VAD flow-rate superimposed to the experimental snapshots acquired using the fast camera. The time of acquisition corresponds to the circles in Figure 3. In all cases, the ventricle slightly contracts and enlarges because of the low ejection fraction (EF=18.2%) imposed by the cam rotation. At the beginning of the diastole, the pressure gradient through the mitral valve increases and the valve opens, thus producing the mitral jet, which gets more intense at the E-wave peak generating a main recirculation in the ventricle. This large-scale vortex further strengthens during the A-wave peak and persists throughout the heart beat according to what observed experimentally in previous in-vitro experiments[18,22]. During systole, the mitral valve closes preventing mitral regurgitation, and the flow can leave the ventricle only through the aortic channel until the initial volume is recovered and the heart beat is completed. We wish to stress that, in Figure 6, the area within the VAD inlet has been blanked since the velocity

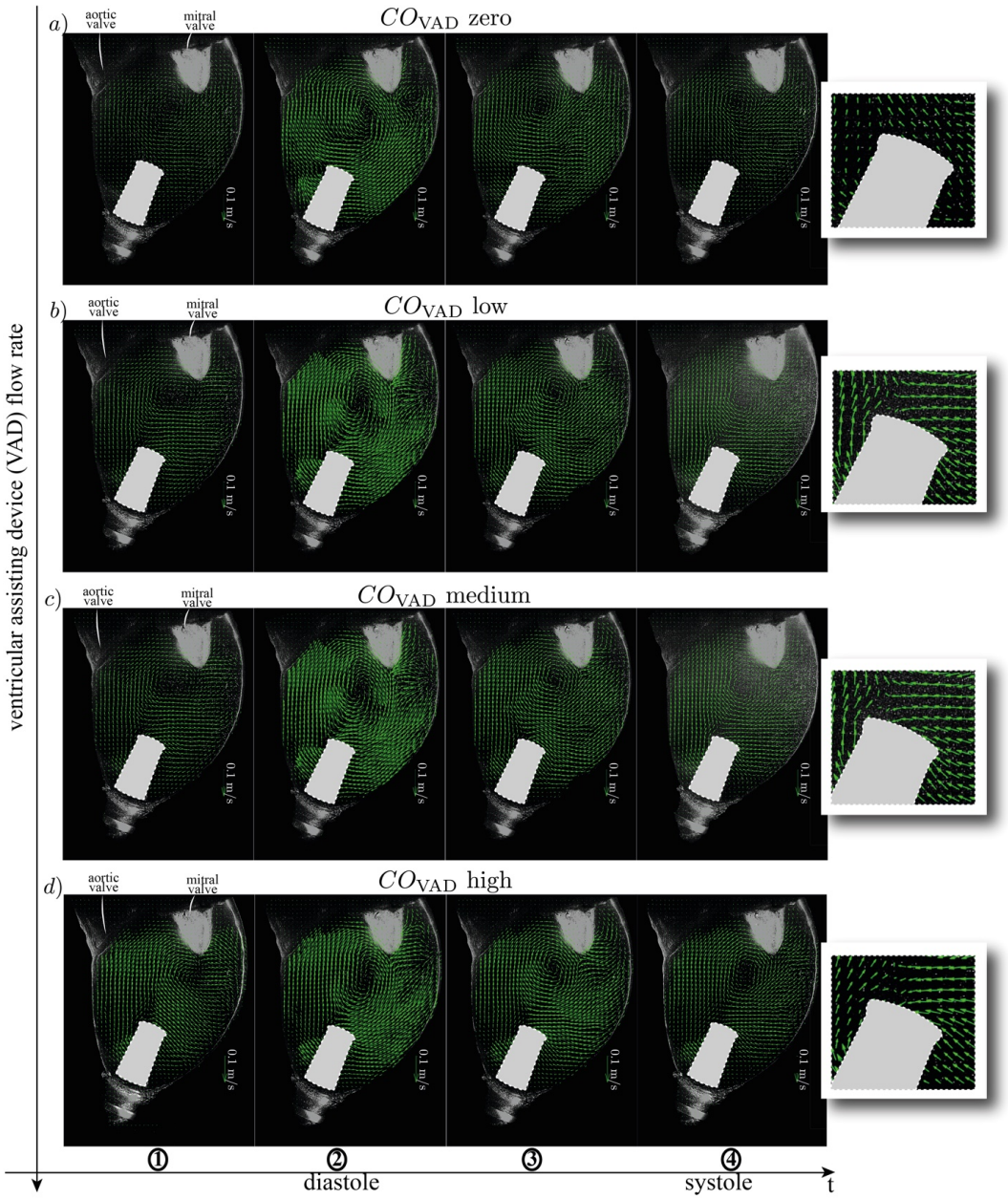

Figure 6: Instantaneous PIV snapshot with superimposed velocity vectors in the $x-z$ plane for VAD regime set to (a) zero (VAD switched off), (b) low, (c) medium, and (d) high flow rate. The time of acquisition corresponds to the circles in Figure 3 and the blanket regions indicate the VAD obstruction within the ventricle. The lateral insets focus on the vectors surrounding the VAD inlet tube.

vectors could not be properly measured; in fact, the position of the very few particles detected in the duct by the fast-camera (see Figure 4b) is distorted by optical refraction. Additionally, the material of the transparent inlet diffuses the laser sheet in the surrounding fluid volume thus illuminating also the particles flowing before (and behind) the inlet itself. As a result, the vectors from the inner and the outer flow were interpolated on the same plane yielding a wrong local flow representation.

As apparent in the lateral inset in Figure 6(a) focusing on the vectors surrounding the VAD inlet tube, when the VAD is turned off ($CO_{\mathrm{VAD}} = 0$) the mass flux inside the tube is null and the velocity vectors are roughly tangent to the tube inlet. On the contrary, when the VAD is active (see insets in Figure 6b-d) the arrows partially point into the VAD inlet thus revealing that fluid particles are leaving the ventricle being sucked by the VAD. In particular, owing to the large scale clockwise circulation, the flow detaches from the right side of the VAD inlet, in analogy with the flow over an open-cavity[27], and enters the tube closer, on average, to its left side. It should be noted that some vectors appear normal to the side wall of the VAD inlet since the finite thickness of the laser sheet, the periodic swinging of the ventricle with respect to the fixed sheet and the three-dimensional structure of the flow around the obstruction, make very difficult to capture the stagnation line where the velocity vectors are null. Furthermore, velocity is measured with respect to a fixed reference frame and all the structure with the fluid therein is moving in time.

Comparison with the hemodynamics in a normal ventricle

Despite the relatively high flow velocities observed during diastole, a low velocity region originates in the ventricle throughout the heart cycle. This area is located at the ventricle apex in the lee of the VAD obstruction that acts as a bluff body, thus generating an intense wake that strongly modifies the ventricular hemodynamics. This phenomenon is well-visible in figure 7(e) where the kinetic energy (KE) in the $x-z$ plane,

$$\mathrm{KE} = 0.5(v_x^2 + v_z^2), \tag{6}$$

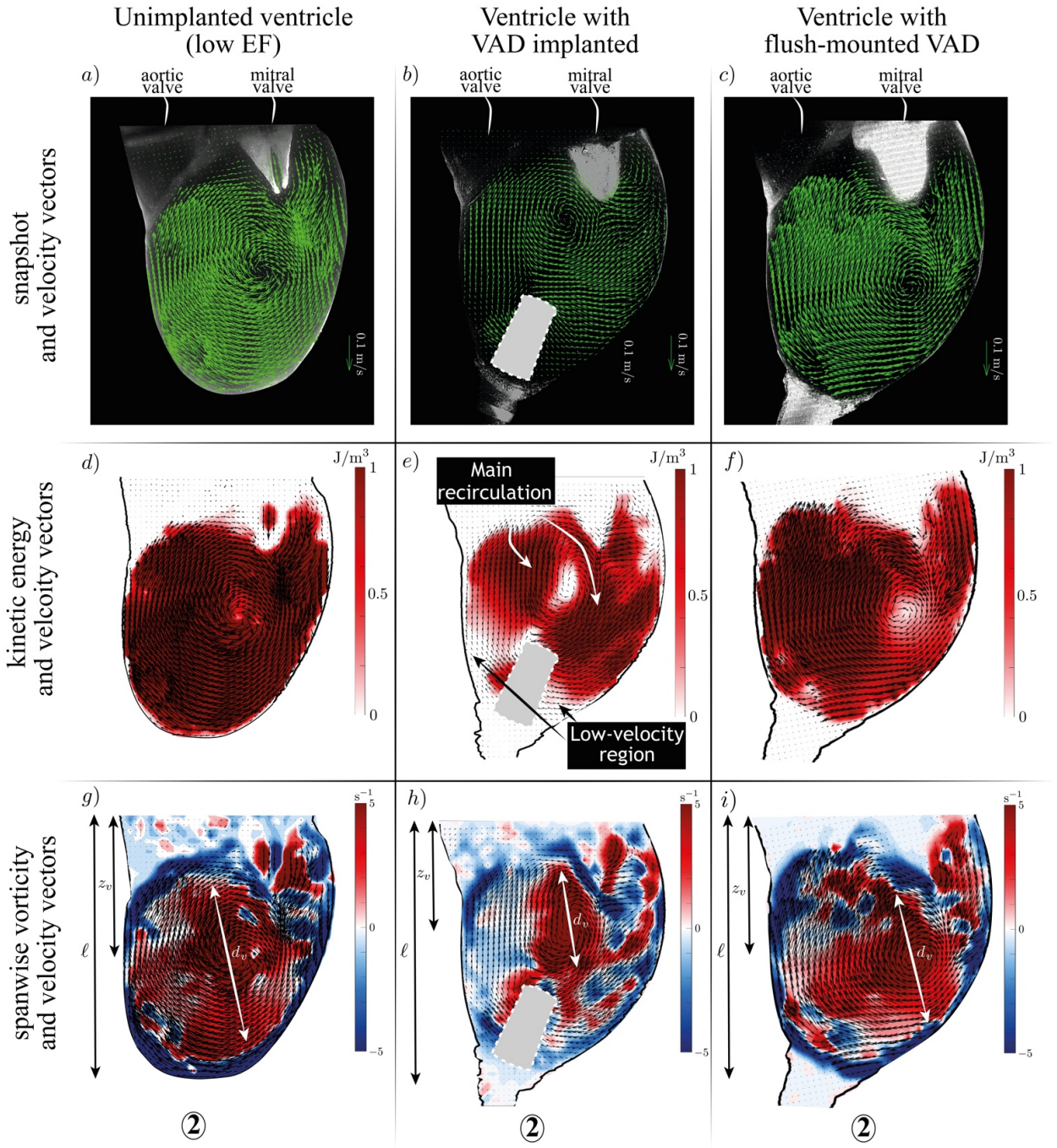

Figure 7: Instantaneous snapshots, kinetic energy (KE) and spanwise vorticity (ζ_y) with superimposed velocity vectors ($v_x\mathbf{e}_x + v_z\mathbf{e}_z$) at the peak diastole are shown in panels (a,d,g) for normal ventricle, in panels (b,e,h) for VAD ventricle with obstruction, and in panels (c,f,i) for flush-mounted VAD. The high VAD flow-rate is considered.

at maximum injection during diastole (E-wave peak) is superimposed to the (v_x, v_z) velocity vectors. It can be seen that the main ventricular circulation induced by the mitral jet produces high KE in the upper part of the ventricle, above the VAD inlet, while the white spot at the center corresponds to the vortex core, which is a minimum of the induced rotational velocity as well-known in vortex dynamics[28]. In contrast, the low KE region (KE more than 70% smaller than in the upper part of the ventricle) at ventricle apex is due to the VAD obstruction that decelerates the fluid particles flowing around the solid obstacle placed in the ventricle. The size of this region scales as the size of the VAD obstruction and hence occupies a significant portion of the ventricle section.

This scenario significantly differs from the dynamics of a normal ventricle, i.e. without VAD implanted, as shown in Figure 7(a,d) where, although the low EF, the KE is more uniformly distributed in the ventricle and fills the whole volume. Also, in this case the minimum of the KE is located at the recirculation core. Importantly, the KE energy in the apical region is 80% higher compared to the case of VAD ventricle and these anomalies between hemodynamics of the assisted ventricle with respect to the normal LV are emphasized when examining the spanwise vorticity component

$$\zeta_y(x,z) = v_{x,z} - v_{z,x}, \tag{7}$$

where the notation $v_{i,j}$ indicates the spatial derivative of the $i-$th velocity component with respect to the direction $j-$th direction. In the case of the ventricle without VAD (Figure 7g), the intraventricular recirculation corresponds to the positive vorticity structure of diameter d_v, of about 60% of the ventricle length ℓ, and occupies a significant fraction of the ventricular volume. Furthermore, the vortex penetrates at a distance $z_v/\ell \sim 55\%$ thus inducing the fluid at the apex to recirculate and to sweep the LV wall. Note that the negative vorticity surrounding the myocardium is the wall vorticity inside the boundary layer, which arises because of the no-slip condition at the solid boundary. In contrast, when a VAD is implanted, the main vortex structure shrinks, $d_v/\ell \lesssim 40\%$ and shifts upwards towards the valvular plane at $z_v/\ell \sim 40\%$. Hence, the vortex induced velocity in the apical region reduces and the ventricle apex becomes stagnant.

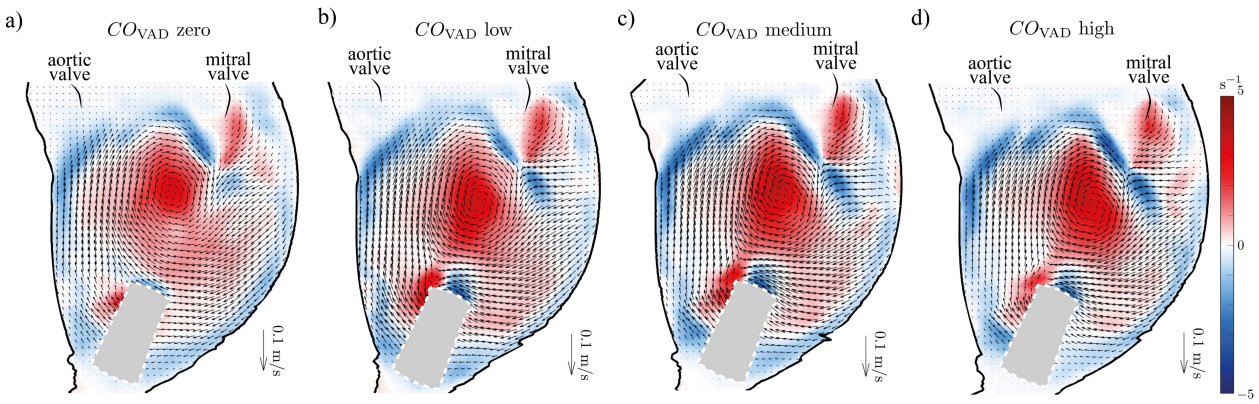

Figure 8: Spanwise vorticity with superimposed velocity vectors for the VAD cardiac output CO_{VAD} set to (a) zero (VAD switched off), (b) low, (c) medium, and (d) high flow rate. Both quantities have been averaged over the ten heart cycles. The dashed profiles indicate the VAD obstruction placed within the ventricle.

Comparison with the hemodynamics of a flush-mounted VAD

In order to further study the effect of VAD on the ventricular hemodynamics, a set of additional experiments has been carried out keeping the continuous VAD suction at the ventricle apex but removing the VAD obstruction. This case-study allows us to measure the hemodynamics corresponding to a very small VAD implant or, more precisely, to a flush-mounted VAD. Figure 7(f) shows that for the high VAD flow-rate at the peak diastole, the KE is better-distributed with respect to the standard VAD case (Figure 7e), similarly to the KE map of the healthy ventricle of Figure 7(d). Furthermore, the size of the main vortex increases to $d_v/\ell \sim 50\%$ with an augmented penetration distance of $z_v/\ell \sim 50\%$: both these parameters are larger than in the VAD-obstructive case. As a result, the formation of a low velocity region close to the apex of the ventricle is prevented when the tube appendage protruding in the ventricle is removed.

This scenario, which has been detailed for the highest VAD flow-rate at the peak diastole, is observed for all considered pumping conditions and throughout the heart cycle as reported in Figure 8, where the spanwise vorticity averaged over ten heart cycles

$$\bar{\zeta}_y(x,z) = \frac{1}{10T}\int_0^{10T} (v_{x,z} - v_{z,x})\mathrm{d}t, \tag{8}$$

is shown. In all cases, due to the VAD obstruction, the main recirculating vortex moves farther from the apex thus inducing the formation of a stagnant region with low velocity close to the VAD inlet tube.

The 'bath-tub vortex' effect

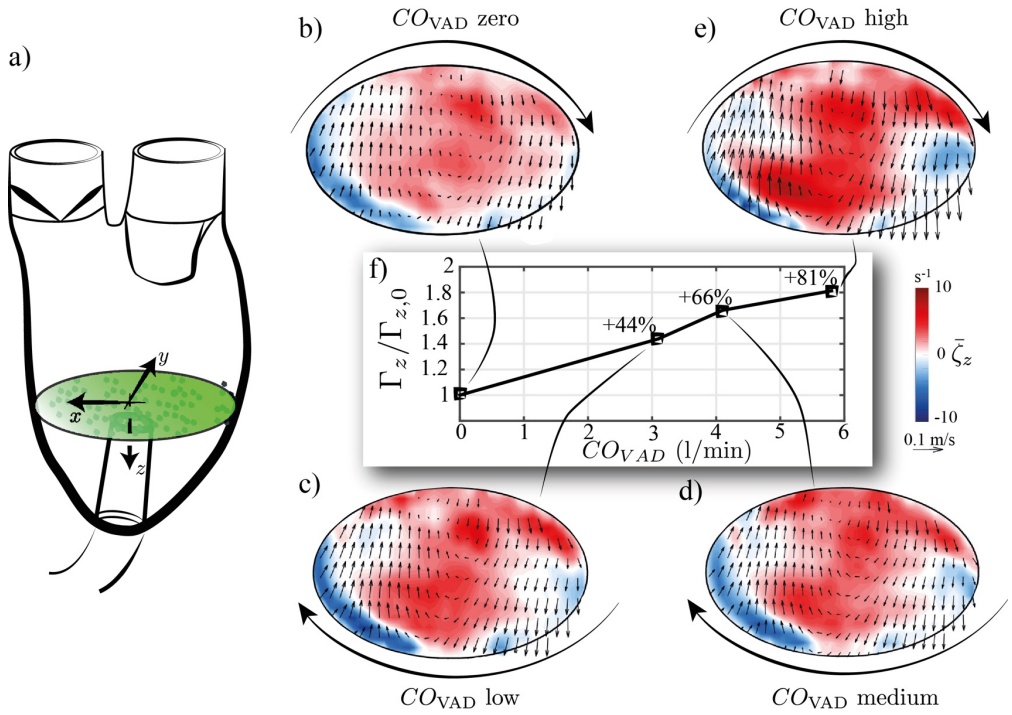

Figure 9: Hemodynamics in the (a) transversal $x-y$ plane above the VAD inlet. Spatial distribution of the vertical vorticity, $\bar{\zeta}_z$, superimposed to the velocity vectors $\delta\bar{v}_x, \delta\bar{v}_y$ (see text) for CO_{VAD} set to (a) zero (VAD switched off), (b) low, (c) medium, and (d) high flow rate. Both quantities have been time averaged over ten heart beats. The corresponding enstrophy (normalized with respect the enstrophy measured with the VAD turned off) is reported in (f) as a function of the VAD cardiac output .

In this section, the hemodynamics in the transversal $x-y$ plane above the VAD inlet (see figure 9a) is studied. To this aim the (vertical) z-component of the vorticity vector time-averaged over ten heart beats

$$\bar{\zeta}_z(x,y) = \frac{1}{10T}\int_0^{10T}(v_{y,z} - v_{x,y})\mathrm{d}t, \tag{9}$$

with t the time and T the beating period, is shown in figure 9(b-e) for four CO_{VAD} values. The positive vorticity distribution (red contours) centered above the VAD inlet corresponds to a

clockwise vortical motion, which is seen to grow with the VAD flow rate. In order to better visualize the swirling nature of the flow, the local velocity field $\bar{v}_x, \bar{v}_y$, can be decomposed as the mean velocity in the $x-y$ plane plus the difference of the local flow velocity with respect to mean velocity:

$$\delta\bar{v}_x(x,y) = \bar{v}_x(x,y) - \int \bar{v}_x \,\mathrm{d}x\mathrm{d}y, \qquad \delta\bar{v}_y(x,y) = \bar{v}_y(x,y) - \int \bar{v}_y \,\mathrm{d}x\mathrm{d}y. \tag{10}$$

The velocity vectors $(\delta\bar{v}_x, \delta\bar{v}_y)$ are superimposed to the vorticity distribution in figures 9(b-e). This velocity field is antisymmetric with respect to the peak vorticity and increases moving away from the vortex core. In particular, by comparing panels (b) and (e), the swirling velocity is significantly higher in the 'high' VAD regime with respect to the case of VAD turned off.

An integral quantity that is typically used to measure the swirling motion of a flow is the enstrophy

$$\Gamma_z = \int \bar{\zeta}_z^2 \,\mathrm{d}x\mathrm{d}y, \tag{11}$$

which is reported in figure 9(f) as a function of the VAD cardiac output. The enstrophy is positively correlated with the VAD flow-rate, thus implying that the VAD suction promotes a vortical motion around the main axis of the ventricle. This result is remnant of the sink flow occurring when water is drained from a tank through a small hole: as the water flows through the bottom hole, the vortex tube is stretched yielding an intense vortical motion whose swirling direction depends on the geometrical asymmetries of the tank[29,28]. This widespread phenomenon occurring at different scales ranging from a domestic sink to dam is called 'bath-tub vortex'. Hence, in a similar fashion, the VAD implant introduces an important modification to the ventricular flow since the bottom suction behaves as a sink that enhances the swirling motion. This bath-tub vortex effect superimposes to the large scale vortex dynamics discussed in the previous section and further modifies the physiological hemodynamics.

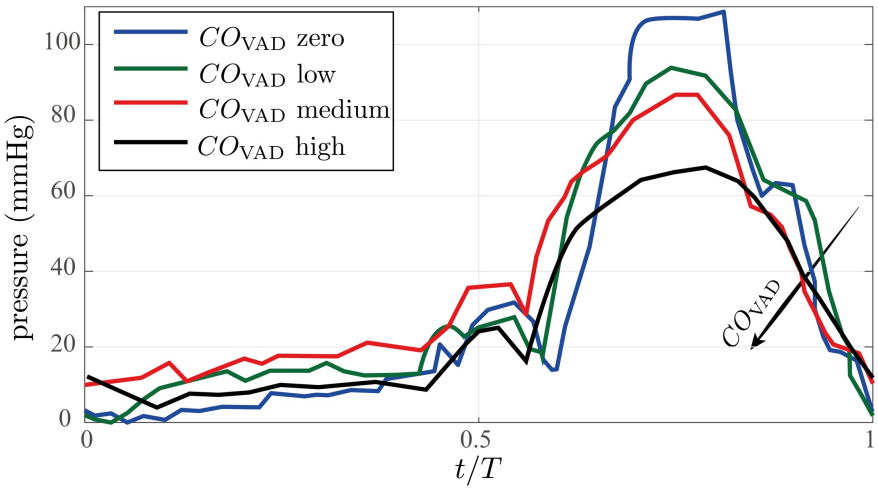

Figure 10: Absolute ventricular pressure phase-averaged over ten heart beats.

VAD modified pressure

We turn now to study the effect of VAD on the ventricular pressure. As mentioned in section 2, the pressure is measured within the sealed box at its bottom, which is below the ventricle. Therefore, the measured value has to be corrected for the hydrostatic pressure difference through the Stevin law. Additionally, the pressure inside the ventricle is higher than the outside value owing to the Laplace correction $\Delta p = \tau / R$, where R is the mean ventricle radius and τ is the ventricle wall tension, which can be evaluated given the time law of the ventricular volume (see Figure 3). The resulting ventricular pressure is reported in Figure 10 for several VAD flow rates, CO_{VAD}. In all cases, the curves start from the reference pressure level (tele-diastolic pressure) during diastole, which then slightly increases during the diastasis. Successively, the maximum pressure is achieved during systolic ejection in the aortic channel. This time behaviour agrees with typical intraventricular pressure measured in-vivo [1,2], and the peak systolic pressure of about 100 mmHg for inactive VAD is in-line with clinical observations for low EF [1]. Importantly, the ventricular pressure decreases when the VAD flow increases and the peak systolic pressure in the high VAD regime decreases up to 40% with respect to the case of inactive VAD. At high CO_{VAD} the systolic pressure peak not only lowers but also broadens becoming less sharp (see the black line). Hence, the suction operated by the VAD affects significantly not only the physiological hemodynamics in the ventricle but it also perturbs the normal pressure field.

These findings agree with previous experimental[30,31] and numerical[32] studies where the left ventricular pressure was seen to decrease along with increased support level of VAD.

3.3 Ventricular dynamics with an implanted assist device

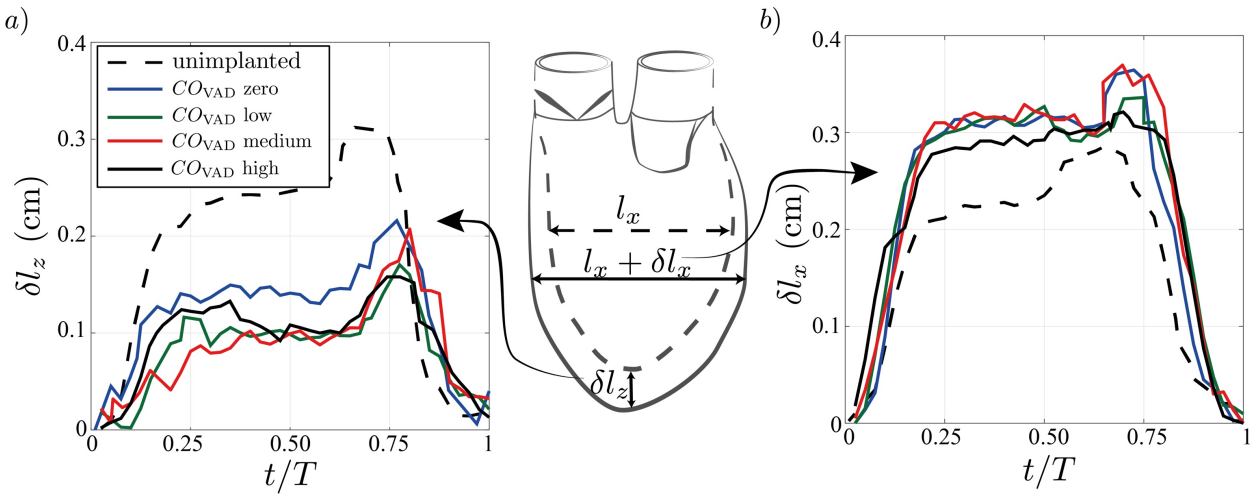

Figure 11: (a) Vertical and (b) horizontal elongation of the ventricle phase-averaged over ten heart beats.

In this section we study the effect of the in-vitro VAD implant on the ventricle dynamics. Figure 11 reports the phase-averaged (a) vertical and (b) horizontal stretching experienced from the ventricle in the case of VAD (solid lines) and unimplanted ventricle (dashed line). In all configurations, both quantities increase during diastole, $0 < t/T < 0.75$, due to ventricle enlargement, and reduce during systole when the ventricle shrinks, $0.75 < t/T < 1$. In particular, the two-steps growth observed for both the vertical δl_z and horizontal δl_x elongations, is due to the ventricle inflow imposed by the cam, which has two peaks (E- and A- waves) as previously shown in figure 3. In the case of VAD ventricle, no significant differences can be observed when the VAD flow is increased from the 'zero' to the 'high' regime and the δl_z, δl_x curves roughly collapse on each other. In contrast, the vertical stretching in the unimplanted case results higher with respect to the VAD ventricle (figure 4b), whereas the horizontal displacement in the VAD case is larger than the one observed in the ventricle dynamics without VAD (figure 4a). It results, therefore, that the by-pass tube mounted in the VAD configurations inhibits

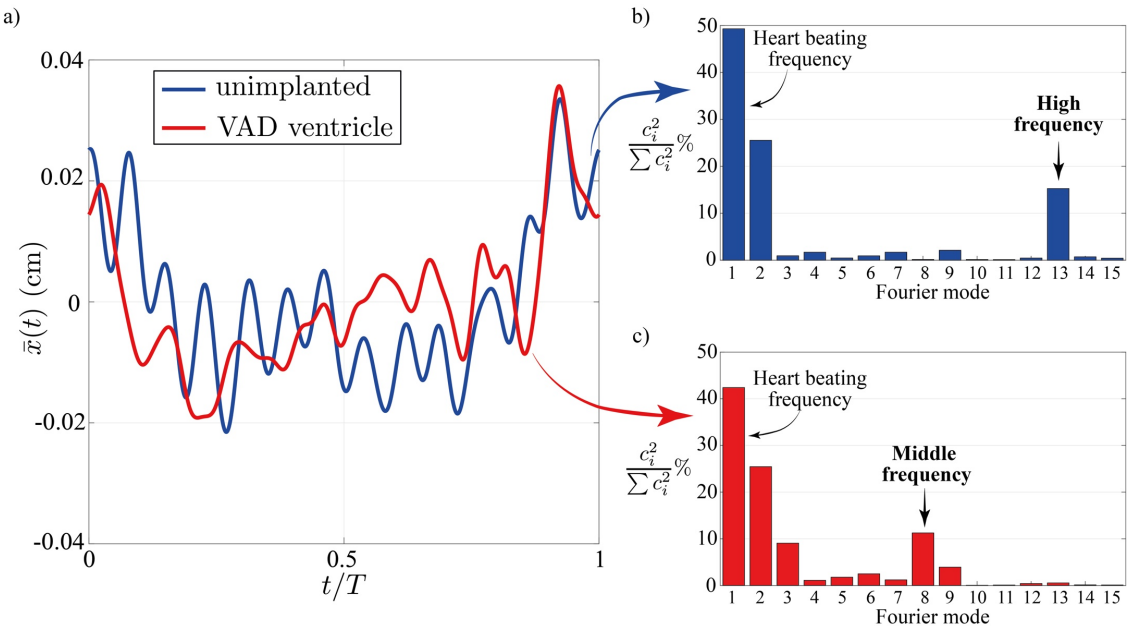

Figure 12: (a) Phase-averaged x-centroid, $\bar{x}$, of the ventricle in the unimplanted (blue) and VAD (red) ventricle with high flow regime. The corresponding relative energy of the Fourier modes are shown in (b) and (c).

the vertical displacement of the ventricle, thus reducing the vertical elongation δl_z with respect to the unimplanted case. However, since the cam motion imposes the same volume variation (and, as a consequence, the same ejection fraction), the horizontal stretching in the VAD case has to be higher with respect to the unimplanted case so that to compensate for the lower δl_z.

Additionally, Figure 12(a) reports the phase averaged displacement of the x-centroid of the unimplanted and VAD ventricle during a heart beat. Although the magnitude of the horizontal oscillations is the same in the two cases, differences are visible in the frequency. More specifically, in both cases a slower modulation (lasting about a heart beat) superimposes over a fast oscillating frequency, which is higher for the unimplanted ventricle with respect to the VAD one. A better insight about the spectral content of the horizontal oscillations is gained by decomposing $\bar{x}(t)$ in superharmonics of the heart beating frequency using Fourier series. The normalized energies of the Fourier modes, which are defined as $c_i^2/\sum c_i^2$ where c_i is the complex Fourier coefficient of the i-mode, are shown in Figure 12(b,c). As anticipated, in both cases the most energetic mode is the fundamental harmonic (mode 1), which can be readily explained by recalling that the system is oscillating at the heart beating frequency imposed by the cam. This mode

nonlinearly forces higher harmonics such as mode 2 that has a relative energy of about 20%. Then, a higher frequency mode, which corresponds to the faster oscillation in Figure 12(a), is well visible in the spectrum and is equal to mode 13 for the unimplanted ventricle and to mode 8 resonates in the VAD case. Hence, the implant of a VAD along with the by-pass tube increases the mass of the system thus lowering its natural frequency, in a similar fashion as a mass-spring oscillator, and yielding a lower transversal mode to resonate. These results about the horizontal oscillation of the VAD ventricle in the 'high' flow rate regime have also been observed for the other VAD pumping regimes, including the case VAD not active ('zero' regime).

4 Discussion

A left ventricular assist device (VAD) is a mechanical pump implanted in patients with heart failure to help their impaired ventricle pump blood throughout the body. The VAD continuously takes blood from the LV apex and delivers it to the ascending aorta, thus decreasing the LV load. The device is typically considered as a "bridge to transplant", i.e. as a temporary therapy. Getting a VAD, however, involves several risks such as blood clots formation due to the presence of the VAD in the ventricle and by the non-pulsatile flow generated by the VAD.

In this work, the modified ventricular hemodynamics due to a VAD implantation has been studied in-vitro using an elastic ventricle that is incorporated (with implanted artificial mitral and aortic valves) into a pulse-duplicator, which generates a realistic pulsatile inflow/outflow through the ventricle corresponding to a weak cardiac output ($CO_{\text{cam}} = 2.4$ l/min). Thereafter, a continuous axial pump is connected at the ventricle apex to mimic a VAD and its effect on the ventricular hemodynamics is investigated as a function of the VAD flow suction using particle image velocimetry (PIV).

We observe that the continuous VAD flow effectively provides unloading on the ventricle and yields the total cardiac output to increase, even if the physiological ventricular hemodynamics is not recovered. Specifically, the results of these experiments suggest that when a VAD is implanted it creates an obstacle to the flow and the main vortex generated from the mitral

jet shrinks and moves farther from the apex towards the valvular plane not reaching the inner walls of the LV down to the apex. As a result, the induced velocity and, therefore, the kinetic energy (KE) around the VAD inlet reduce. We have found that monitoring the ventricular KE is a convenient way of understanding LV efficiency and whether adequate hemodynamics is achieved. In this respect, we have observed experimentally that, despite the EF below 20%, the mitral jet originating in an unimplanted ventricle induces a rather efficient ventricular recirculation, which properly washes the myocardium including the apical region and yields a more uniformly distributed intraventricular KE with respect to the one measured in a VAD ventricle. In order to better understand the effect of the VAD inlet design on the ventricular hemodynamics, dedicated experiments with a flush-mounted VAD have been carried out. It has been found that removing the VAD obstruction in the ventricle prevents the formation of the low velocity region close to the apex and favors a more uniform KE field, similar to the one observed in the unimplanted case. Furthermore, both the size of the recirculation vortex and its penetration distance from the valvular plane increase respectively of 50% and 40%. Hence, our experiments prove that the modified KE distribution measured in the VAD ventricle is due to the obstruction of the VAD inlet rather than to the VAD suction itself. Indeed, the portion of the VAD inserted into the LV behaves as a bluff body, which creates a large wake (of the size of the body diameter) decelerating the intraventricular flow and preventing the development of physiological hemodynamics. This scenario is quite robust and is observed throughout the heart cycle and for several VAD flow rates. Importantly, we have found that a flush-mounted VAD yields a more efficient intraventricular hemodynamics similar to that of a healthy ventricle.

Additionally, the investigation of the hemodynamics in the transversal plane placed above the VAD inlet reveals as the suction operated by the VAD significantly increases the mean vortical motion around the ventricle axis. This result has been shown to be in close analogy with the bath-tub vortex, i.e. the strong vortical motion manifesting when a tank is emptied through a hole. It has to be remarked, however, that in the familiar case of a tank emptied from its bottom, the flow is driven by the hydrostatic pressure, whereas in the case of VAD ventricle the by-pass flow is generated by the continuous VAD suction. Nevertheless, the swirling motion originated

by the VAD further modifies the intraventricular hemodynamics with respect to healthy conditions.

It is well known that an important consequence of an abnormal intraventricular hemodynamics is a change of the values and spatial distribution of the wall shear stress (WSS) that, in turn, can induce inflammatory reactions or tissue remodelling via mechanotransduction processes: this is certainly another important aspect that should be evaluated when assessing the performance of VAD devices. Unfortunately, in the present study, accurate WSS measurements would require dedicated experiments focussing only on a small region of the ventricle wall, so to obtain the fine PIV resolution needed to capture the wall gradients (of the order of one tenth of the Stokes boundary layer, $\delta = \sqrt{2\nu/\omega} = 1.2$ mm, which corresponds to 120 μm). Achieving the needed resolution, however, would prevent the description of the entire ventricular hemodynamics that is the main aim of this work. Nevertheless, even if we can not directly measure WSS, we can speculate about them with the support of our experimental results. We expect the VAD to have two main opposite effects on the WSS: the weakened ventricular recirculation, due to VAD obstruction, reduces the WSS in the $x-z$ plane, while, in contrast, the enhanced swirling motion originated by the VAD suction (the bath-tub vortex effect) increases the WSS in the azimuthal direction. However, since the trabeculae of the endocardium are mainly aligned with the z–direction, the two WSSs are not equivalent and the missing 'sweeping action' of the WSS in the $x-z$ plane might be another reason for the anticoagulant therapy needed by VAD implanted patients.

A physiological hemodynamics in the ventricle is of paramount importance for the patient health. Indeed, the abnormal blood circulation induced by VAD implant can cause clots formation in the stagnant region at the apex which, in turn, can further damage the LV or eventually break off into the system circulation causing stroke or ischemia. Studies on the physiological effects of VADs show that these devices can lead to an increase in degradation of the aortic wall tissue, thrombosis and higher degrees of hemolysis, which are important physiological factors to be considered for VAD therapy[33]. In this framework, a better understanding of the hemodynamics perturbed by the VAD, as done here, could help rationalizing these clinical observations

and develop more effective and less invasive devices to favor long-term use of VAD. As resulting from our work, changes in KE and flow mapping can be excellent tools to provide evidence of LV disfunction, enabling earlier medical intervention.

As also found in previous in-vitro experiments[30,31] and numerical simulations[32], our experiments confirm that the VAD implant not only affects the hemodynamics, but also the ventricle pressure which is seen to decrease monotonically as long as the VAD cardiac output is increased. Specifically, for the highest VAD regime the peak systolic pressure decreases of about 40% with respect to the case of VAD turned off. The intraventricular pressure modification has a tremendous impact on patient health because it drives the remodelling of the ventricular myocardium. Moreover, it affects the opening/closing cycle of the aortic valve and increases the risk of aortic insufficiency, i.e. the aortic valve does not completely close during diastole thus originating a leaking of blood from the aorta into the left ventricle. Degenerative aortic valve changes are indeed frequently observed after long-term VAD support[34] and, besides that, more than 60% of patients supported by VAD manifest commissural fusion of the aortic valve[35,36]. These observations may be important in the use of these pumps as long-term destination therapy.

Regarding the ventricle dynamics, the VAD implant along with the by-pass tube, is seen to reduce the vertical elongation of the ventricle during diastole with respect to the case of an unimplanted ventricle. As a consequence, the horizontal elongation increases in the VAD case in order to retrieve the same volume variation of the unimplanted one. On the other hand, the diastolic ventricle expansion does not depend on the magnitude of the by-pass flow rate as comparable vertical and horizontal elongations are observed for the VAD regimes considered in the experiments. Interestingly, since the VAD increases the mass of the ventricle, it also modifies the natural frequencies of the system and lowers the frequency of the oscillating mode that resonates during the heart cycle.

We conclude by mentioning that, despite the geometry and nondimensional numbers are set to match as closely as possibly a biological ventricle, the model only embeds some representative features of what physiologically occurs in the human heart. For instance, in the current

study the aortic valve is modeled using a simple check-valve and, although the low EF prevents the mitral leaflets from everting inside the mitral channel, *cordae tendinae* and the papillary muscles connected to the mitral valve leaflets are not present. Furthermore, the internal surface of the silicone model is smooth unlike the endocardium tessellated by irregular corrugations, called *trabeculae*. Additionally, the mitral annulus in the experiment is planar and rigid, while in the real heart the shape changes during the heartbeat and assumes an elliptic shape. Another relevant difference is that the ventricle dynamics is driven here by the pressure forces exerted by the surrounding fluid triggered by the piston that are inevitably normal to the ventricle surface, whereas the active force contraction of the myocardium is the result of an electrical stimulus propagating in the myocytes and is non-isotropic since it is oriented along the local fiber direction. This mechanism can not be reproduced experimentally when passive elastic materials are used to fabricate the ventricle. Nevertheless, laboratory experiments have the advantage of being run in controllable and repeatable conditions and they also allow for the use of velocimetry techniques such as the PIV suitable to investigate the complex structure of the flow. Moreover, the resulting hemodynamics is realistic and closer to clinical experience especially in the diastolic phase where the myocardium relaxes due to the inflow through the mitral channel. A natural follow-up of this work would be to investigate the hemodynamics of left ventricles with VAD implanted in-vivo, using for instance echocardiographic-PIV[37,38], which is a fairly novel noninvasive technique where acoustic reflections from ultrasound contrast agents are tracked to measure instantaneous blood velocity within the heart or arteries. This approach would allow to verify that the modified vortex dynamics due to VAD implant studied in this work effectively happens in patients and monitor how this depends on the VAD size.

References

1. Katz A. M.. Physiology of the Heart. Lippincott Williams & Wilkins. 2010.

2. Runge, M.S. and Ohman, M. . Netter's cardiology. Saunders/Elsevier. 2010.

3. Picano, E.. Stress echocardiography. Heidelberg, Springer. 2003.

4. Trulock EP, Christie JD, Edwards LB, Boucek MM, Aurora P, Taylor DO, Dobbels F, Rahmel AO, Keck BM, Hertz MI. Registry of the International Society for Heart and Lung Transplantation: twenty-fourth official adult lung and heart-lung transplantation reportâĂŤ2007. The Journal of heart and lung transplantation. 2007; 26(8): 782-95.

5. Ventricular Assist Devices (VADs). Texas Heart Institute. https://www.texasheart.org/heart-health/heart-information-center/topics/ventricular-assist-devices/. Accessed July 19, 2018.

6. Timms, D.. A review of clinical ventricular assist devices. Medical engineering & physics. 2011; 33(9):1041-1047.

7. Lahpor, J.R.. State of the art: implantable ventricular assist devices. Current opinion in organ transplantation. 2009; 14(5): 554-559.

8. Westaby, S., Katsumata, T., Houel, R., Evans, R., Pigott, D., Frazier, O.H. and Jarvik, R.. Jarvik 2000 heart: potential for bridge to myocyte recovery. Circulation; 1998; 98(15): 1568-1574.

9. Frazier, O.H., Myers, T.J., Westaby, S. and Gregoric, I.D.. Use of the Jarvik 2000 left ventricular assist system as a bridge to heart transplantation or as destination therapy for patients with chronic heart failure. Annals of surgery. 2003; 237(5); 631.

10. Stainback, R.F., Croitoru, M., Hernandez, A., Myers, T.J., Wadia, Y. and Frazier, O.H.. Echocardiographic evaluation of the Jarvik 2000 axial-flow LVAD. Texas Heart Institute Journal. 2005; 32(3), 263.

11. Xie A, Phan K, Yan TD. Durability of continuous-flow left ventricular assist devices: a systematic review. Ann Cardiothorac Surg. 2014; 3(6): 547-556.

12. Allen, J.G., Weiss, E.S., Schaffer, J.M., Patel, N.D., Ullrich, S.L., Russell, S.D., Shah, A.S. and Conte, J.V.. Quality of life and functional status in patients surviving 12 months after left ventricular assist device implantation. The Journal of Heart and Lung Transplantation. 2010; 29(3): 278-285.

13. Mizuguchi, K., Damm, G., Benkowsky, R., Aber, G., Bacak, J., Svjkovsky, P., Glueck, J., Takatani, S., NosÃl', Y., Noon, G.P. and DeBakey, M.E.. Development of an axial flow ventricular assist device: in vitro and in vivo evaluation. Artificial Organs,1995;19(7):653-659.

14. Wheeldon, D.R., LaForge, D.H., Lee, J., Jansen, P.G., Jassawalla, J.S. and Portner, P.M.. Novacor left ventricular assist system long-term performance: comparison of clinical experience with demonstrated in vitro reliability. Asaio Journal. 2002; 48(5):546-551.

15. Timms, D., Fraser, J., Hayne, M., Dunning, J., McNeil, K. and Pearcy, M.. The BiVACOR rotary biventricular assist device: concept and in vitro investigation. Artificial Organs. 2008; 32(10): 816-819.

16. John, R.. Current axial-flow devicesâĂŤthe HeartMate II and Jarvik 2000 left ventricular assist devices. In Seminars in thoracic and cardiovascular surgery. WB Saunders. 2008; 20(3): 264-272).

17. Cenedese, A., Prete, Z. D., Miozzi, M., Querzoli. G.. A laboratory investigation of the flow in the left ventricle of a human heart with prosthetic, tilting-disk valves. Experiments in Fluids. 2005; 39:322-335.

18. Fortini, S., Querzoli, G., Espa, S., Cenedese, A.. Three-dimensional structure of the flow inside the left ventricle of the human heart. Experiments in Fluids. 2013; 54:1-9.

19. Querzoli, G., Fortini, S., Cenedese, A.. Effect of the prosthetic mitral valve on vortex dynamics and turbulence of the left ventricular flow. Physics of Fluids (1994-present). 2010; 22:041901.

20. Karmonik, C., Partovi, S., Loebe, M., et al. Computational fluid dynamics in patients with continuous-flow left ventricular assist device support show hemodynamic alterations in the ascending aorta. The Journal of Thoracic and Cardiovascular Surgery. 2014;147(4).

21. Blausen.com staff. Medical gallery of Blausen Medical 2014. WikiJournal of Medicine. 2014; 1 (2).

22. Meschini, V., De Tullio, M., Querzoli, G., & Verzicco, R. Flow structure in healthy and pathological left ventricles with natural and prosthetic mitral valves. Journal of Fluid Mechanics. 2018; 834: 271-307.

23. Siginer, D.A., De Kee, D. and Chhabra, R.P. eds., 1999. Advances in the flow and rheology of non-Newtonian fluids (Vol. 8). Elsevier.

24. Westaby, S., Anastasiadis, K., Wieselthaler, G. M.. Cardiogenic shock in ACS. Part 2: role of mechanical circulatory support. Nature Reviews Cardiology. 2012 Apr;9(4):195.

25. Baldwin, J. T., Adachi, I., Teal, J., Almond, C.A., Jaquiss, R.D., Massicotte, M.P., Dasse, K., Siami, F.S., Zak, V., Kaltman, J.R., Mahle, W.T.. Closing in on the PumpKIN trial of the Jarvik 2015 ventricular assist device. InSeminars in Thoracic and Cardiovascular Surgery: Pediatric Cardiac Surgery Annual 2017 Jan 1 (Vol. 20, pp. 9-15). WB Saunders.

26. Thielicke, W. and Stamhuis, E. J.: PIVlab - Time-Resolved Digital Particle Image Velocimetry Tool for MATLAB. 2014.

27. Barbagallo, A., Sipp, D., Schmid, P.J.. Closed-loop control of an open cavity flow using reduced-order models. Journal of Fluid Mechanics. 2009; 641:1-50.

28. Saffman, P.G.. Vortex dynamics. Cambridge university press; 1992.

29. Sibulkin, M.. A note on the bathtub vortex. Journal of Fluid Mechanics. 1962; 14:21-24.

30. Tuzun, E., Pennings, K., van Tuijl, S., de Hart, J., Stijnen, M., van de Vosse, F., de Mol, B. and Rutten, M.. Assessment of aortic valve pressure overload and leaflet functions in an ex vivo beating heart loaded with a continuous flow cardiac assist device. European Journal of Cardio-Thoracic Surgery. 2013; 45(2), pp.377-383.

31. Tuzun, E., Rutten, M., Dat, M., Van De Vosse, F., Kadipasaoglu, C. and De Mol, B.. Continuous-flow cardiac assistance: effects on aortic valve function in a mock loop. Journal of Surgical Research. 2011; 171(2), pp.443-447.

584 32. Zhang, Q., Gao, B., Yu, C.. The Effects of Left Ventricular Assist Device Support Level on
585 the Biomechanical States of Aortic Valve. Medical science monitor: international medical
586 journal of experimental and clinical research. 2018;24:2003.

587 33. Healy, A.H., McKellar, S.H., Drakos, S.G., Koliopoulou, A., Stehlik, J., Selzman, C.H.. Physi-
588 ologic effects of continuous-flow left ventricular assist devices. The Journal of surgical re-
589 search. 2016; 202(2):363-371.

590 34. Hata, H., Fujita, T., Ishibashi-Ueda, H., Nakatani, T., Kobayashi, J.. Pathological analysis of
591 the aortic valve after long-term left ventricular assist device support. European Journal of
592 Cardio-Thoracic Surgery, 2014; 46: 193-97

593 35. Connelly, J. H., Abrams, J., Klima, T., Vaughn, W. K., Frazier, O. H.. Acquired commissural
594 fusion of aortic valves in patients with left ventricular assist devices. The Journal of heart
595 and lung transplantation. 2003 Dec 1;22(12):1291-5.

596 36. Banchs, J.E., Dawn, B., Abdel-Latif, A., Qureshi, A., Agrawal, N., Bouvette, M., Stoddard,
597 M.F.. Acquired aortic cusp fusion after chronic left ventricular assist device support. Journal
598 of the American Society of Echocardiography. 2006 Nov 1;19(11):1401-e1.

599 37. Kheradvar, A., Houle, H., Pedrizzetti, G., Tonti, G., Belcik, T., Ashraf, M., Lindner, J.R.,
600 Gharib, M., Sahn, D.. Echocardiographic particle image velocimetry: a novel technique for
601 quantification of left ventricular blood vorticity pattern. Journal of the American Society of
602 Echocardiography. 2010.

603 38. Faludi, R., Szulik, M., Dhooge, J., et al. Left ventricular flow patterns in healthy subjects and
604 patients with prosthetic mitral valves: An in vivo study using echocardiographic particle
605 image velocimetry. The Journal of Thoracic and Cardiovascular Surgery. 2010;139(6):1501-
606 1510.

607 39. Benjamin, E.J., et al.; on behalf of the American Heart Association Council on Epidemiol-
608 ogy and Prevention Statistics Committee and Stroke Statistics Subcommittee. Heart disease

609 and stroke statistics 2018 update: a report from the American Heart Association [published
610 online ahead of print January 31, 2018]. Circulation.